 CMES, vol.102, no.5, pp.345-358, 2014

A (Constrained) Microstretch Approach in Living Tissue Modeling: a Numerical Investigation Using the Local Point Interpolation – Boundary Element Method

Jean-Philippe Jehl[1] **and Richard Kouitat Njiwa**[2]

Abstract: Extended continuum mechanical approaches are now becoming increasingly popular for modeling various types of microstructured materials such as foams and porous solids. The potential advantages of the microcontinuum approach are currently being investigated in the field of biomechanical modeling. In this field, conducting a numerical investigation of the material response is evidently of paramount importance. This study sought to investigate the potential of the (constrained) microstretch modeling method. The problem's field equations have been solved by applying a numerical approach combining the conventional isotropic boundary elements method with local radial point interpolation. Our resulting numerical examples demonstrated that the model is a good candidate for the mechanical modeling of living tissues.

Keywords: Micromorphic, Constrained microstretch, Isotropic BEM, Meshfree strong form.

1 Introduction

It is becoming increasingly clear that the microstructure of material must be taken into account when establishing its corresponding constitutive equation. Mechanical behavior modeling considers the microstructural information of a material either implicitly or explicitly. Living tissue, such as heart tissue, is non homogeneous with a complex micro-organization. In this context, it is not easy to apply multi-scale modeling or classical mathematical homogenization approaches; phenomenological approaches are still required. It is for this reason that we chose to continue the work of Rosenberg and Cimrman (2003) and investigate the applicability of microcontinuum approaches in this field.

[1] Université de Lorraine, Institut Jean Lamour - Dpt N2EV - UMR 7198 CNRS Parc de Saurupt, CS 14234, F-54042 Nancy Cedex, Jean-Philippe.Jehl@ijl.nancy-universite.fr

[2] Université de Lorraine, Institut Jean Lamour - Dpt N2EV - UMR 7198 CNRS Parc de Saurupt, CS 14234, F-54042 Nancy Cedex, Richard.Kouitat@ijl.nancy-universite.fr

The theory behind using micromorphic media, as described by Eringen and Suhubi (1964), is that it enables us to capture the impact of the microstructure on the overall response of the material. For a full description: a material point of a micromorphic medium possesses twelve degrees of freedom: the three traditional components of displacement and nine components of a micro-deformation tensor. The material is typically specialized depending on the salient microscopic motions.

When the material point of the medium can rotate and stretch, the medium is known as a microstretch material. In the constrained microstretch medium, the material point can only dilate or contract, and is known as a microdilatation medium, a definition already applied to model foam and some porous media [Ramézani, Steeb and Jeong (2012)]. The literature on microstretch media is not extensive. It is, in fact, difficult to understand and qualify the responses of this type of media using conventional mechanical tests. We believe that numerical experiments are extremely useful in this field. On account of this, we have opted to investigate the response of a 3D (constrained) microstretch medium to loading. Our study presented herein is essentially numerical and based on a specifically developed numerical tool. First of all, we present the governing equations of a microstretch medium. Then, we describe the adopted numerical method, called the "local point interpolation – boundary element method" (LPI-BEM). Finally, the numerical results are presented. Particular attention was paid to verify the model's capacity to represent the mechanical behavior of living tissue, such as heart tissue.

2 Governing Equations

In the theory of microstretch medium occupying the domain Ω with boundary Γ, the material point x is attached to a triad of directors that can rotate and stretch. The material point possesses seven degrees of freedom: the three components of the traditional displacement vector, the three components of a microrotation vector, and the scalar microdilatation. The field equations governing this type of medium when under quasi-static evolution without external body loads are [Iesan and Pompei (1995)]:

$$\sigma_{ji,j}(x) = 0 \tag{1}$$

$$m_{ji,j}(x) + \varepsilon_{ijk}\sigma_{jk}(x) = 0 \tag{2}$$

$$s_{k,k}(x) - p(x) = 0 \tag{3}$$

In these equations, $\sigma_{ij}(x)$ represents the stress tensor, $m_{ij}(x)$ the couple stress tensor, $s_k(x)$ the vector of internal hypertraction, and the scalar $p(x)$ is the generalized internal body load. The latter can be viewed as an internal pressure. Next we considered the case of a quasi-homogeneous and isotropic solid, for which producing

the following corresponding constitutive relations are as follows:

$$\sigma_{ij}(x) = \lambda \varepsilon_{rr} \delta_{ij} + 2(\mu + \kappa)\varepsilon_{ij} - \kappa u_{i,j} + \kappa \varepsilon_{jik} \varphi_k + \eta(x)\psi \delta_{ij} \tag{4}$$

$$m_{ij} = \alpha \omega_{rr} \delta_{ij} + (\beta + \gamma)\omega_{ij} + (\beta - \gamma)(\varphi_{i,j} - \varphi_{j,i})/2 \tag{5}$$

$$s_k = a\psi_{,k} \tag{6}$$

$$p(x) = \eta(x)\varepsilon_{rr} + b\psi \tag{7}$$

Where ψ is the micro-stretch function, u_i the macroscopic displacement vector, and φ_i the microscopic rotation vector.

$$\varepsilon_{ij} = (u_{i,j} + u_{j,i})/2$$

$$\omega_{ij} = (\varphi_{i,j} + \varphi_{j,i})/2.$$

λ and μ are the Lamé constants; α, β, γ, and κ the micropolar constants; $\eta(x)$, a, and b the microstretch elastic constants.

It should be noted that, in our selected model, only parameter $\eta(x)$ could vary within the medium.

With n_j as the outward normal vector on the boundary, the tractions acting at a regular point of the boundary are given by:

$$t_i = \sigma_{ji} n_j, \quad m_i = m_{ji} n_j, \quad s = s_j n_j \tag{8}$$

The material parameters must fulfil the following constraints:

$$b(3\lambda + 2\mu + \kappa) - 3\eta^2 \geq 0, \quad 2\mu + \kappa \geq 0, \quad \kappa \geq 0, \quad a \geq 0,$$
$$b \geq 0, \quad 3\alpha + \beta + \gamma \geq 0, \quad \beta + \gamma \geq 0, \quad \gamma - \beta \geq 0.$$

3 Solution Method

In the case of linear problems with a well-established analytical fundamental solution, the boundary element method has already proven highly efficient. In our study, no fundamental solution of the field equations existed; the boundary element method (BEM) was found to lose its principal appeal, namely the reduction of the problem dimension by one, due to traditional volume cells being needed in the "field boundary element method". In order to overcome this obstacle, a number of strategies have been proposed, such as the dual reciprocity method (DRM) or radial integration method (RIM), which enable the conversion of volume integrals into surface ones. In recent years, a large number of researchers have invested in the development of so-called meshless or meshfree methods. Among the various meshless approaches, the local point interpolation method is highly appealing

on account of how simple it is to implement. This approach falls in accuracy in the presence of Neumann boundary conditions, which are almost an inevitability when solving solid mechanic problems. Liu *et al.* (2001) have suggested a way to circumvent this difficulty by adopting the "weak-strong-form local point interpolation" method. In a recent publication, Kouitat Njiwa (2011) proposed a novel strategy that combines the best elements of both the conventional BEM and local point interpolation methods. This LPI-BEM approach has proved efficient in the context of anisotropic elasticity [Kouitat Njiwa (2011)], piezoelectric solids [Thurieau, Kouitat Njiwa and Taghite (2012)], and nonlocal elasticity [Schwartz, Niane and Kouitat Njiwa (2012)]. We adopted this method in our study, detailing below the principal steps followed in the context of a microstretch medium. It should also be mentioned that a solution procedure using the finite element method was also presented by Kirchner and Steinmann (2007).

Our calculations were based on the assumption that the kinematical primary variables are the sum of a complementary part and a particular term. Namely: $u_i = u_i^H + u_i^P$, $\varphi_i = \varphi_i^H + \varphi_i^P$, and $\psi = \psi^H + \psi^P$.

The complementary fields satisfied the following homogeneous equations:

$$\bar{G}_u \left[\Delta u_i^H + \frac{1}{1-2\tilde{\nu}_u} u_{j,ji}^H \right] = 0, \quad \bar{G}_\varphi \left[\Delta \varphi_i^H + \frac{1}{1-2\tilde{\nu}_\varphi} \varphi_{j,ji}^H \right] = 0, \quad a\psi_{,kk}^H = 0. \tag{9}$$

The new parameters in equations (9) were defined as:

$$\bar{G}_u = \mu + \kappa, \quad \tilde{\nu}_u = \frac{\lambda}{2(\lambda+\mu+\kappa)}, \quad \bar{G}_w = \frac{1}{2}(\gamma+\beta), \quad \tilde{\nu}_w = \frac{\alpha}{\beta+\gamma+2\alpha}.$$

Equations (9) were solved by the conventional boundary element method, thus producing the following systems of equations:

$$[H_u]\{u^H\} = [G_u]\{t^H\}, [H_\varphi]\{\varphi^H\} = [G_\varphi]\{m^H\}, [H_\psi]\{\psi^H\} = [G_\psi]\{s^H\}. \tag{10}$$

The particular fields solved:

$$\bar{G}_u \left[\Delta u_i^P + \frac{1}{1-2\tilde{\nu}_u} u_{j,ji}^P \right] - \kappa u_{j,ji} + \kappa \varepsilon_{ijk} \varphi_{k,j} + (\eta\psi)_{,i} = 0 \tag{11}$$

$$\bar{G}_\varphi \left[\Delta \varphi_i^P + \frac{1}{1-2\tilde{\nu}_\varphi} \varphi_{j,ji}^P \right] + (\beta-\gamma)\frac{(\varphi_{j,ij} - \varphi_{i,jj})}{2} - \kappa\varphi_i - \kappa\varepsilon_{ijk} u_{k,j} = 0 \tag{12}$$

$$a\psi_{,kk}^P - b\psi - \eta u_{r,r} = 0 \tag{13}$$

The tractions at a regular point on the boundary were written as:

$$t_i = t_i^H + t_i^P + \delta t_i \text{ with } t_i^A = \left(\lambda \varepsilon_{rr}^A \delta_{ij} + 2(\mu+\kappa)\varepsilon_{ij}^A\right) n_j \,(A = H \text{ or } P)$$
$$\text{and } \delta t_i = \left(-\kappa u_{i,j} + \kappa \varepsilon_{jik}\varphi_k + \eta\,\psi\delta_{ij}\right) n_j \tag{14}$$

$$m_i = m_i^H + m_i^P + \delta m_i \text{ with } t_i^A = \left(\alpha \omega_{rr}^A \delta_{ij} + (\beta+\gamma)\omega_{ij}^A\right) n_j \,(A = H \text{ or } P)$$
$$\text{and } \delta m_i = (\beta-\gamma)(\varphi_{j,i} - \varphi_{i,j}) n_j/2 \tag{15}$$

$$s = s^H + s^P \text{ with } s^A = a\psi_{,j}^A n_j \,(A = H \text{ or } P) \tag{16}$$

Following this, we then considered the solution of equations (11-13), using a local radial point collocation method. In this method [Liu and Gu (2001)], a field $\omega(x)$ was approximated as:

$$\omega(x) = \sum_{i=1}^{N} R_i(r)\, a_i + \sum_{j=1}^{M} p_j(x)\, b_j$$

with the following constraints: $\sum_{i=1}^{N} p_j(x)\, a_i = 0$, $j = 1-M$ and $i = 1-N$.

Here $R_i(r)$ is the selected radial basis functions, N the number of nodes in the neighborhood (support domain) of point x, and M the number of monomial terms in the selected polynomial basis $P_j(x)$.

Coefficients a_i and b_j could be determined by enforcing the approximation to be satisfied at the N centers. Following some algebraic manipulations, coefficients a_i and b_j could be expressed in terms of the field nodal values, and the interpolation could be written in the following compact form:

$$\omega^h(x) = [\varphi(x)]\left\{\omega_{/L}\right\} \tag{17}$$

When adopting interpolation (17) for all kinematical fields, at a given collocation center, the following were obtained:

$$[B(\nabla)]^T [C_u][B(\nabla)][\tilde{\varphi}]\left\{u_{/L}^P\right\} + \kappa[\tilde{\varphi}_1]\left\{u_{/L}\right\}$$
$$+ \kappa[\tilde{\varphi}_2]\left\{\varphi_{/L}\right\} + \{\nabla\}[\tilde{\varphi}_3][\eta]\left\{\psi_{/L}\right\} = \{0\}$$
$$[B(\nabla)]^T \left[C_\varphi\right][B(\nabla)][\tilde{\varphi}]\left\{\varphi_{/L}^P\right\} + \kappa[\hat{\varphi}_0]\left\{\varphi_{/L}\right\}$$
$$+ (\beta-\gamma)[\hat{\varphi}_1]\left\{\varphi_{/L}\right\} + \kappa[\hat{\varphi}_3]\left\{u_{/L}\right\} = \{0\}$$
$$a\{\nabla\}^T\{\nabla\}\left\{\breve{\Phi}\right\}^T\left\{\psi_{/L}^P\right\} - b\left\{\breve{\Phi}_1\right\}^T\left\{\psi_{/L}\right\} - \{\nabla\}^T[\tilde{\varphi}][\eta]\left\{u_{/L}\right\} = 0$$

In the above, $\{\nabla\} = (\partial/\partial x, \partial/\partial y, \partial/\partial z)^T$, $\{z\} = (z_1, z_2, z_3)^T$,

$$[B(z)] = \begin{bmatrix} z_1 & 0 & 0 & z_2 & z_3 & 0 \\ 0 & z_2 & 0 & z_1 & 0 & z_3 \\ 0 & 0 & z_3 & 0 & z_1 & z_2 \end{bmatrix}^T$$

Matrix B was given in terms of vector $z = (z_1, z_2, z_3)^T$ and matrix C was the Voigt representation of the elasticity tensor.

On collection of the above equations for all the internal collocation centers, taking the assumption that the particular integrals are identically zero at all boundary points, the following forms of systems of equations were obtained:

$$\left\{u^P\right\} = [A_u]\{u\} + [B_u]\{\varphi\} + [C_u]\{\psi\} \tag{18}$$

$$\left\{\varphi^P\right\} = \left[A_\varphi\right]\{\varphi\} + \left[B_\varphi\right]\{u\} \tag{19}$$

$$\left\{\psi^P\right\} = \left[A_\psi\right]\{\psi\} + \left[B_\psi\right]\{u\} \tag{20}$$

Following a similar strategy, the tractions at the boundary points could be written in the following forms:

$$\{t\} = \left\{t^H\right\} + [AK_{uu}]\{u\} + \left[AK_{u\phi}\right]\{\varphi\} + \left[AK_{u\psi}\right]\{\psi\}$$

$$\{m\} = \left\{m^H\right\} + \left[AK_{\varphi u}\right]\{u\} + \left[AK_{\varphi\varphi}\right]\{\varphi\}$$

and $\{s\} = \left\{s^H\right\} + \left[AK_{\psi u}\right]\{u\} + \left[AK_{\psi\psi}\right]\{\psi\}$

After conducting some algebraic manipulations, the final coupled systems of equations were of the following forms:

$$[\bar{H}_u]\{u\} + \left[H_{u\varphi}\right]\{\varphi\} + \left[H_{u\psi}\right]\{\psi\} = [G_u]\{t\} \tag{21}$$

$$\left[\bar{H}_\varphi\right]\{\varphi\} + \left[H_{\varphi u}\right]\{u\} = \left[G_\varphi\right]\{m\} \tag{22}$$

$$\left[\bar{H}_\psi\right]\{\psi\} + \left[H_{\psi u}\right]\{u\} = \left[G_\psi\right]\{s\} \tag{23}$$

Particularly worthy of mention, the final equations contained similar boundary primary variables and internal kinematic unknowns to those of a traditional BEM. Boundary conditions could be taken into account as in standard practice and the resulting system of equations was solved by a standard direct solver. It must be mentioned that equations 9 could be solved using radial functions with local boundary integral equation. This new and simple numerical scheme was recently introduced in reference [Sellountos, Polyzos and Atluri (2012)].

4 Numerical examples

In our work, we applied the multi-quadrics radial basis functions as follows: $R_i(r) = \left(r_i^2 + c^2\right)^q$, where $r_i = \|x - x_i\|$ and c and q were known as shape parameters. Shape parameter c was taken proportionally to minimum distance d_0, defined as the maximum value among the minimum distances in the x, y, and z directions between collocation points.

Firstly, we had to validate the proposed tool on a cubic specimen. The boundary of the cube was subdivided into 24 nine-node quadrilateral elements. The boundary nodes were supplemented by 27 internal collocation centers.

The first material parameters used in the simulation have been presented in Table 1.

Table 1: Material parameters of the microstretch medium

λ	μ	η	κ	α	β	γ	a	b
18000	-14680	-0.037	38370	-12000	12000	36000	1.83	0.037

As expected, for the pure tension case, the micro-rotation equaled zero within the specimen, while the microstretch function was uniform. For example, at the top surface of the specimen, the axial displacement and microstretch function were, respectively,: $u_z = 0.396410210^{-6}$ and $\psi = 0.158732910^{-5}$. Figure 1 presents the displacement vector field and its component in the loading direction. Where η was decreased to -0.37 (a variation by factor 10), the macroscopic displacement was slightly modified, while the microstrectch function increased by factor 10. These results remained practically unchanged when the multiquadrics shape parameters varied in range $[-2;2]$ for q and range $\left[10^{-4};10^{-1}\right]$ for c.

The numerical approach proposed in our paper proved effective in the context of tension loading due to the numerical solutions being analytical in nature. The next step of the analysis consisted of submitting the cubic specimen to shearing. The microstretch function was expected to be zero throughout the specimen while the microrotation was activated. Our numerical results aligned with this requirement. These results were unaffected when the multi-quadrics shape parameters were varied. Our numerical approach also proved effective for this type of loading.

A careful selection of material parameters enabled an adequate simulation of auxetic material response. Auxetics are materials that have a negative Poisson's ratio. These materials expand under tensile loading. When the parameters outlined in Table 2 were adopted, auxetic behavior was observed (Fig.2).

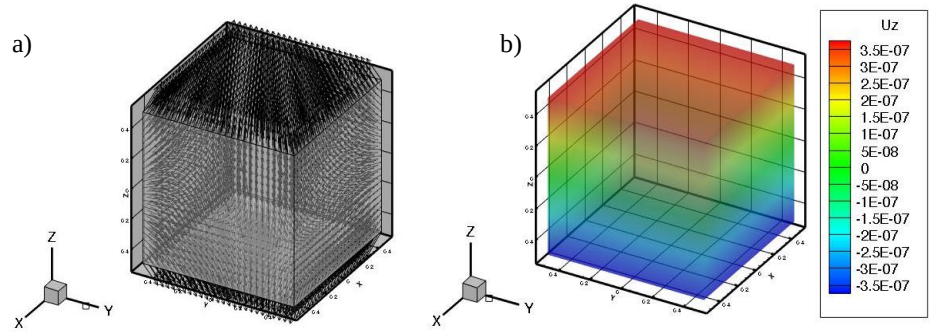

Figure 1: Cubic specimen a) Displacement vector under pure tension b) Displacement component in the loading direction.

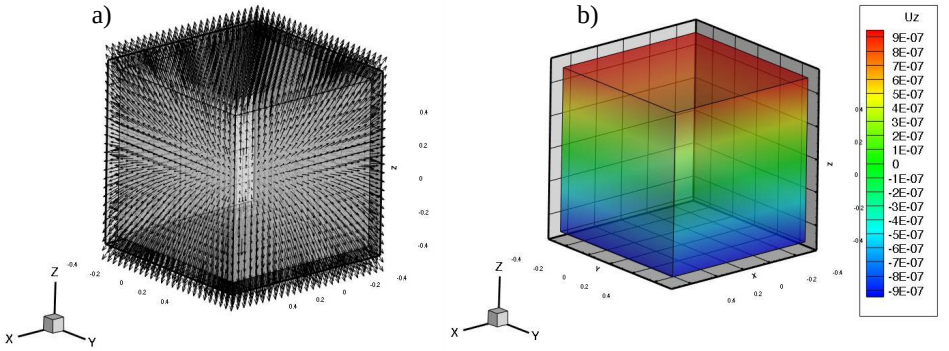

Figure 2: Cubic specimen a) Displacement vector under pure tension b) Displacement in the loading direction.

Table 2: Material parameters of a microstretch medium (auxetic response)

λ	μ	η	κ	α	β	γ	a	b
18000	-14680	-19000	38370	-12000	12000	36000	1.83	18000

At the (0.5, 0.5, 0.5) coordinate point, the axial and lateral displacements and microstretch function were, respectively: $u_z = 0.95612610^{-6}$, $u_x = 0.401210^{-6}$, and $\psi = 0.371210^{-5}$ (Figure 2).

Next, we considered the left ventricle as modeled as a tubular specimen (see Figure 3). [Johnston (2003)]. Due to the loading of the specimen, the simulation could be restricted to a situation of a constrained microstretch medium, or microdilatation medium. In addition, with respect to myocardial infarction, we believed that the most salient microscopic feature was the material point's ability "breath".

The tubular specimen had an exterior radius of 0.75mm, a thickness of 0.5mm, and was 1.25mm long. This specimen was loaded by 10^{-2}GPa pressure on its outer boundary. The material parameters adopted were: μ = 0.85 GPa, λ = 3.4 GPa, a = 26 kN, b = 26 GPa, and η = -10.15 GPa. The results presented were obtained with the boundary of the specimen subdivided into 288 nine-node boundary elements, supplemented by 432 internal collocation centers.

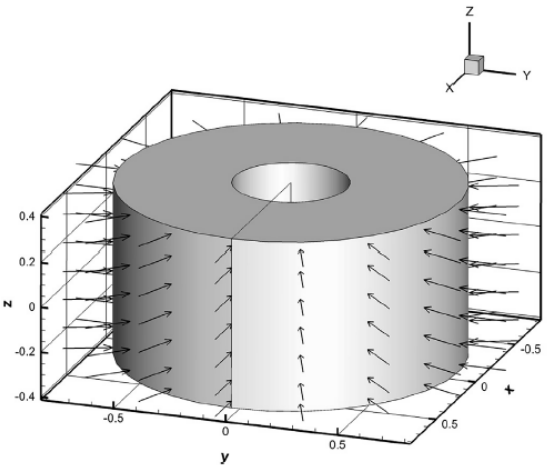

Figure 3: Geometry and loading of the tubular specimen.

Figure 4 displays the deformation of a cross section of the cylinder. It should be noted that, under this loading state and with regards to displacement field, all cross sections of the cylinder are identical.

These results should correlate with the left ventricular ejection fraction (LVEF), namely the ratio between the volume ejected by the left ventricle (end-systolic volume) and the initial volume (end-diastolic volume). This measurement holds clinical significance as it demonstrates the heart's capacity to adequately pump blood,

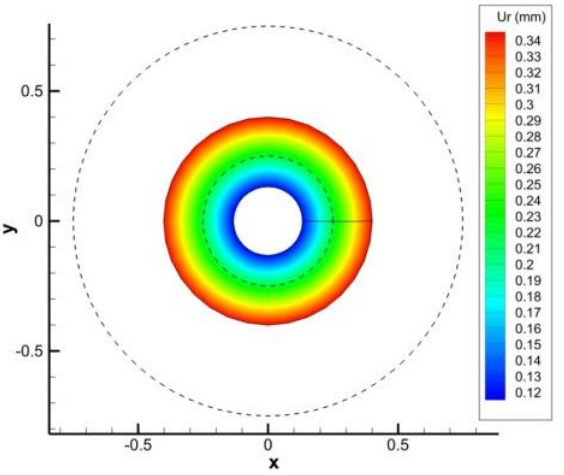

Figure 4: Radial displacement in a cross section of the cylinder with microdilatation.

and therefore oxygen, around the body. Certain studies ([Nardinocchi et al. (2012); Cohn et al. (1993); Juillière et al. (1997); Hallstrom et al. (1995)]) have used LVEF values as indicators for heart failure prognosis. P. Curtis *et al.* (2003) stated in their work that as the LVEF rose from 15 to 45%, mortality rates fell linearly. Once the 45% marker was surpassed, the mortality rate appeared no longer affected. The ejection fraction calculated for the cases presented in Figure 1 was 84.7%. This criterion provided a solid foundation for evaluating this model's capacity to analyze the mechanical behavior of the left ventricle. Henceforth in this study, the material with the above parameters is called the safe specimen.

Our next step was to consider a sample covering a small zone containing varying η parameter values. This zone was intended as a representation of a post-infarction necrotic area. We first positioned it near the outer boundary of the tube. Figure 5 displays a representation of the deformation in the middle of the sample, demonstrating that it was no longer uniform. In accordance with our expectations, the results indicated a significant regression in the LVEF, of approximately 48%, when parameter η of the necrotic zone was far removed from that of the healthy organ. This was due to a slight narrowing of the cylinder's interior and slight shortening of the tube itself. We also succeeded in reducing the axial deformation, as was achieved by Cho *et al.* in their clinical study [Cho (2009)] comprising heart failure patients with accompanied fall in LVEF. This constitutes yet further confirmation of this model's great potential for modeling cardiac tissue behavior.

The necrotic zone was then positioned in proximity to the inner boundary of the tube, at which point we were particularly focused on the contractility of the neighboring points to this zone (Fig. 6). In contrast to our findings in the previous cases, a large zone on the opposite side of the necrotic area here revealed a significant reduction in contractility. This result is in line with observations made by Reimer *et al.* in their series of experiments [Reimer (1977)], describing a phenomenon of tissue necrosis spreading from the endocardium to the epicardium or, in layman's terms, from the interior to the exterior of the heart.

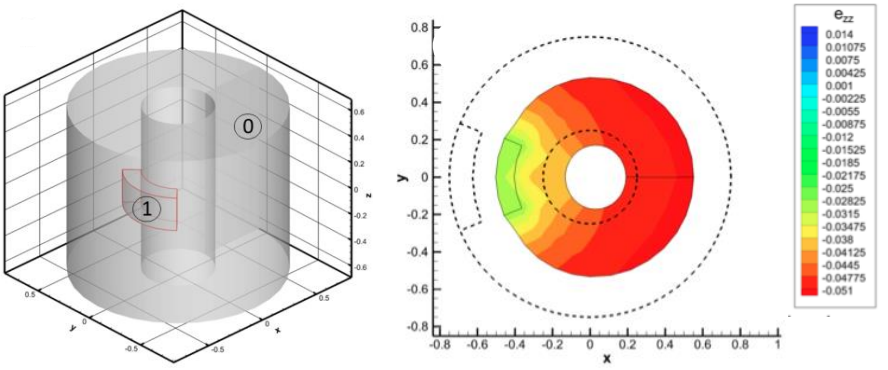

Figure 5: Axial deformation in a cross section of the cylinder, η = -10.15 GPa in the "safe" zone (0) and η = -2 GPa in the affected zone (1).

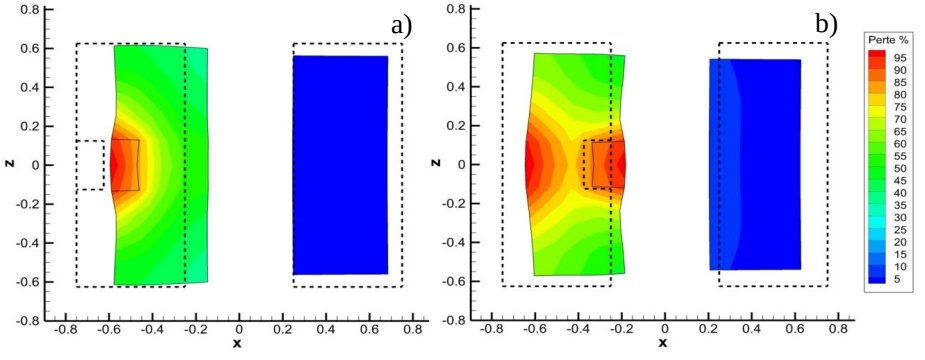

Figure 6: Loss of dilatation: affected zone initially in the proximity of the outer boundary a) or the inner boundary b).

5 Conclusion

This primarily numerical work illustrated the great potential of the "local point interpolation – boundary element" method for addressing problems relating to the microstretch modeling of living tissue. The LPI-BEM has already proven effective and accurate for anisotropic, nonlocal, and piezoelectric elasticity. The method couples conventional isotropic BEM with local radial point interpolation applied to strong-form differential equations. The solution procedure required only minor modifications to the existing BEM code.

Our results presented here testify to this approach's capacity to deal with localized non homogeneity, such as that found in a necrotic area. Considering myocardial infarction, we observed a reduction in axial deformations following the introduction of an infarct zone, as well as the development of an infarction spreading from the endocardium to the epicardium. An affected zone positioned in proximity to the exterior of the heart was found to exact less reductive effect on the muscle's capacity to contract than that of a zone positioned close to the inner wall. Following on from this study, another study is scheduled to continue with our investigations, taking into account the conical geometry of the left ventricle in addition to including the anisotropy of the physical parameters into the model.

References

Cho, G.-Y.; Marwick, T. H.; Kim, H.-S.; Kim, M.-K.; Hong, K.-S.; Oh, D.-J. (2009): Global 2-Dimensional Strain as a New Prognosticator in Patients With Heart Failure. *Journal of the American College of Cardiology*, vol. 54, issue 7, pp. 618–624.

Cohn, J. N.; Johnson, G. R.; Shabetai, R.; Loeb, H.; Tristani, F.; Rector, T.; Smith, R.; Fletcher, R. (1993): Ejection fraction, peak exercise oxygen consumption, cardiothoracic ratio, ventricular arrhythmias, and plasma norepinephrine as determinants of prognosis in heart failure. The V-HeFT VA Cooperative Studies Group. *Circulation*, vol. 87, no. 6, pp. VI5–16.

Curtis, J. P.; Sokol, S. I.; Wang, Y.; Rathore, S. S.; Ko, D. T.; Jadbabaie, F.; Portnay, E. L.; Marshalko, S. J.; Radford, M. J.; Krumholz, H. M. (2003): The association of left ventricular ejection fraction, mortality, and cause of death in stable outpatients with heart failure. *Journal of the American College of Cardiology*, vol. 42, issue 4, pp. 736–742.

Eringen, A. C.; Suhubi, E. S. (1964): Nonlinear theory of simple micro-elastic solids – I. *International Journal of Engineering Science*, vol. 2, no 2, pp. 189–203.

Hallstrom, A.; Pratt, C. M.; Greene, H. L.; Huther, M.; Gottlieb, S.; DeMaria,

A.; Young, J. B. (1995): Relations between heart failure, ejection fraction, arrhythmia suppression and mortality: analysis of the Cardiac Arrhythmia Suppression Trial. *J. Am. Coll. Cardiol.*, vol. 25, issue 6, pp. 1250–1257.

Iesan D.; Pompei, A. (1995): On the equilibrium theory of microstretch elastic solids. *International Journal of Engineering Science*, vol. 33, no 3, pp. 399–410.

Johnston, P. R. (2003): A cylindrical model for studying subendocardial ischaemia in the left ventricle. *Mathematical Biosciences*, vol. 186, issue 1, pp. 43–61.

Juillière, Y.; Barbier, G.; Feldmann, L.; Grentzinger, A.; Danchin, N.; Cherrier, F. (1997): Additional predictive value of both left and right ventricular ejection fractions on long-term survival in idiopathic dilated cardiomyopathy. *Eur. Heart J.*, vol. 18, issue 2, pp. 276–280.

Kirchner, N.; Steinmann, P. (2007): Mechanics of extended continua: modeling and simulation of elastic microstretch materials. *Computational Mechanics*, vol. 40, no 4, pp. 651–666.

Kouitat Njiwa, R. (2011): Isotropic-BEM coupled with a local point interpolation method for the solution of 3D-anisotropic elasticity problems. *Engineering Analysis with Boundary Elements*, vol. 35, no 4, pp. 611–615.

Liu, G. R.; Gu, Y. T. (2001): A local radial point interpolation method (LRPIM) for free vibration analyses of 2-D solids. *Journal of Sound and Vibration*, vol. 246, no 1, pp. 29–46.

Nardinocchi, P.; Puddu, P. E.; Teresi, L.; Varano, V. (2012): Advantages in the torsional performances of a simplified cylindrical geometry due to transmural differential contractile properties. *European Journal of Mechanics* - A/Solids, vol. 36, pp. 173–179.

Ramézani, H.; Steeb, H.; Jeong, J. (2012): Analytical and numerical studies on Penalized Micro-Dilatation (PMD) theory: Macro-micro link concept. *European Journal of Mechanics - A/Solids*, vol. 34, pp. 130–148.

Reimer, K. A.; Lowe, J. E.; Rasmussen, M. M.; Jennings, R. B. (1977): The wavefront phenomenon of ischemic cell death. 1. Myocardial infarct size vs duration of coronary occlusion in dogs. *Circulation,* vol. 56, issue 5, pp. 786–794.

Rosenberg, J.; Cimrman, R. (2003): Microcontinuum approach in biomechanical modeling. *Mathematics and Computers in Simulation*, vol. 61, pp. 249–260

Schwartz, M.; Niane, N. T.; Kouitat Njiwa, R. (2012): A simple solution method to 3D integral nonlocal elasticity: Isotropic-BEM coupled with strong form local radial point interpolation. *Engineering Analysis with Boundary Elements*, vol. 36, no 4, pp. 606–612.

Sellountos, E. J.; Polyzos, D.; Atluri, S.N. (2012): A New and Simple Meshless

LBIE-RBF Numerical Scheme in linear Elasticity. *Computer modeling in engineering and Sciences*, vol. 89, no. 6, pp. 513–551.

Thurieau, N.; Kouitat Njiwa, R.; Taghite, M. (2012): A simple solution procedure to 3D-piezoelectric problems: Isotropic BEM coupled with a point collocation method. *Engineering Analysis with Boundary Elements*, vol. 36, no 11, pp. 1513–1521.